Relative pressure estimation from velocity measurements in blood flows: state-of-the-art and new approaches

Cristobal Bertoglio, Rodolfo Núñez, Felipe Galarce, David Nordsletten, Axel Osses

Relative pressure estimation from velocity measurements in blood flows: state-of-the-art and new approaches

Cristóbal Bertoglio[1], Rodolfo Núñez[1], Felipe Galarce[1,2], David Nordsletten[3], and Axel Osses[1]

[1]Center for Mathematical Modeling, Universidad de Chile, Chile
[2]Civil Engineering School, P. Universidad Católica de Valparaiso, Chile
[3]Department of Biomedical Engineering, King's College of London, UK

May 30, 2016

Abstract

The pressure gradient across stenotic blood vessels is an important clinical index for diagnosis of the pathological severity of the cardiovascular disease. While the clinical gold standard for its measurement is invasive catheterization, Phase-Contrast MR-imaging has emerged as a promising tool for enabling a non-invasive quantification of the relative pressures, by linking the (highly spatially resolved) velocity measurements with the relative pressure via the Navier-Stokes equations. In this work we first provide a review of current methods for relative pressure estimation, propose new ones and perform a theoretical bias analysis for all of them. Finally, we compare the precision and robustness all these approaches on numerical examples using subsampled and noisy synthetic data verifying the theoretical findings.

1 Introduction

Aortic coarctation is a congenital disease consisting of a stenosis of the aorta near its arc. Pressure difference between before and after the stenosis is a standard clinical measurement that serves to asses the severity of the pathology. It may be performed several times during diagnosis and follow up [15], in order to determine the need of a surgical intervention and/or a more intensive follow up.

The most reliable procedure in clinical practice to obtain peak instantaneous pressure gradient involves the measurement of relative pressure invasively via catheterization, which has restricted indications and should be avoided unless non-invasive evaluations (like ultrasound) are inconclusive or discordant with clinical findings [13].

Alternatively, Phase-Contrast Magnetic Resonance Imaging (PC-MRI) allows to obtain three-dimensional, time-resolved measurements of the velocity field, allowing visualization of complex blood flow patterns in large vessels and the heart [10]. Typical PC-MRI spatial and temporal resolutions go from 1.5 to 3 mm^3 and $20-40$ ms, respectively [5]. Hence, it has been natural to postulate methods to compute the relative pressures using these measured velocities and the Navier–Stokes equations.

First in [7, 6], and revisited recently in the context of finite elements in [8], a relative pressure field was reconstructed by directly plugging the velocity measurements into a Navier–Stokes equation, and solving a Poisson equation for the pressure. This approach is usually denoted by Pressure Poisson Estimator (PPE).

Recently in [11], the authors proposed to solve a Stokes problem, which they called STE, by adding a divergence-free vector to the Navier–Stokes residual, which results in a mixed problem for this vector and the pressure to be estimated. In the tests presented in [11], turning out to overperform the PPE in terms of precision.

Also very recently in [4], relative pressure and velocity measurements were proposed to be related by using the classical integral energy balance of the incompressible Navier–Stokes equations, denoted as WERP. This has the advantage that only few integrals have to be evaluated, making it computationally faster than the PPE and STE. However, the authors indicated some potential drawbacks: (i) the measurement terms are squared, amplifying the noise, in particular for small in-/outflows, and (ii) it cannot be applied for simultaneous estimation of relative pressure in multiple outlet geometries.

The purpose of this manuscript is twofold. First, we propose modifications to the STE and WERP in order to improve their estimation precision. Secondly, we formulate an alternative integral approach of the momentum balance for estimating relative pressures. We show that this overcomes the drawbacks of the WERP in several numerical examples using synthetic data. We also compute the statistical bias of all methods, what to the authors best knowledge has not yet been reported.

The rest of this paper is organized as follows. In Section 2 we set up the pressure estimation problem. In Section 3 we revisit the state-of-the-art methods mentioned above. In Section 4 we propose new pressure estimation approaches. In Section 5 we perform a theoretical bias analysis for all the methods. In Section 6 we test and compare all methods using synthetic data, including sensitivity to noise, spatial and temporal subsampling. Finally in Section 7 we discuss the results and draw some conclusions and perspectives.

2 The relative pressure estimation problem

Let us consider an incompressible, Newtonian fluid in a bounded domain $\Omega \subset \mathbb{R}^d$, $d = 2, 3$, modeled by the incompressible Navier–Stokes equations with the velocity $\boldsymbol{u}(t) : \Omega \to \mathbb{R}^d$ and the pressure $p(t) : \Omega \to \mathbb{R}$, $t \in [0, T]$:

$$\begin{cases} \rho \partial_t \boldsymbol{u} + \rho(\boldsymbol{u} \cdot \boldsymbol{\nabla})\boldsymbol{u} - \mu \Delta \boldsymbol{u} + \boldsymbol{\nabla} p = \boldsymbol{0} \quad \text{in} \quad \Omega \times [0, T], \\ \boldsymbol{\nabla} \cdot \boldsymbol{u} = 0 \quad \text{in} \quad \Omega \times [0, T] \end{cases} \tag{1}$$

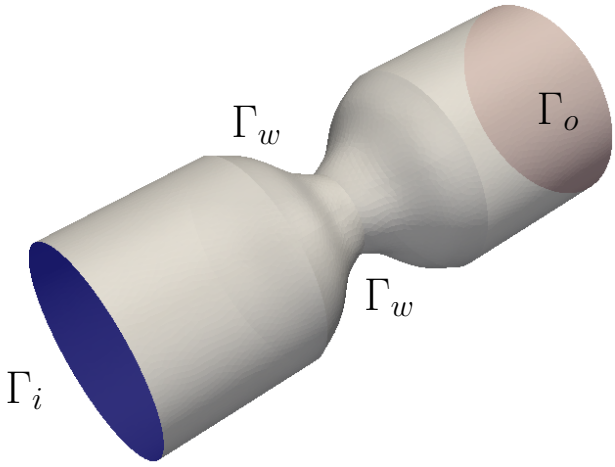

Figure 1: Aortic geometry with 60% coarctation.

where ρ is the density and μ the dynamic viscosity. We also assume that the boundary of Ω given by $\partial\Omega := \Gamma = \Gamma_i \cup \Gamma_o \cup \Gamma_w$, with $\Gamma_i \cap \Gamma_o = \emptyset$. Γ_i is the inlet boundary (typically the one proximal to the heart), Γ_o the outlet (distal) boundary and Γ_w is the arterial wall boundary, as in Figure 1. The task of the relative pressure estimation is to compute:

$$\delta p = \frac{1}{|\Gamma_i|}\int_{\Gamma_i} p - \frac{1}{|\Gamma_o|}\int_{\Gamma_o} p \tag{2}$$

given (perturbed) measurements of $\boldsymbol{u}$ in Ω.

As is obtained in Phase-Contrast MRI, we will assume that the velocity measurements are available at h-spaced discrete points of the domain Ω, but we will be able to reconstruct them everywhere by: (a) computing a mesh $\mathcal{T}_h$ of the domain Ω using the measurement locations, and then (b) interpolating the velocity components at every point in Ω using simple linear piecewise finite element basis functions. Additionally, we will asume that these space-discrete measurements will be available at N discrete measurement times $t^1, ..., t^N$ at a constant time interval τ. We will denote the measurements as $\boldsymbol{u}_m^1, ..., \boldsymbol{u}_m^N \in [\mathcal{P}_{1,h}]^d$, with $\mathcal{P}_{1,h}$ the usual piecewise continuous linear polinomial finite element space.

Moreover, for further analysis we assume that the measurements include a random, additive perturbation with respect to the ground truth velocity, i.e. $\boldsymbol{u}_m^n = \boldsymbol{u}_h^n + \boldsymbol{\varepsilon}^n$, with $\boldsymbol{u}_h^n \in [\mathcal{P}_{1,h}]^d$ a spatial subsampling of the true field $\boldsymbol{u}$ into $[\mathcal{P}_{1,h}]^d$ at observation time t^n, and $\boldsymbol{\varepsilon}^n \in [\mathcal{P}_{1,h}]^d$ a discrete noise field, with all degrees-of-freedom independently identically distributed (i.i.d.) following a normal distribution $\mathcal{N}(0, \sigma^2)$.

3 State of the art of estimation methods

In this section, we overview the mathematical formulations of the currently available methods to estimate relative pressure. We start with the *Poisson Pressure Estimator (PPE)*, which is the oldest and most popular, however, the less precise and robust with respect to spatial subsampling of the data in our numerical examples. We continue with the *Stokes estimator (STE)* and then with the *Work-Energy Relative pressure estimator (WERP)*, which

were very recently introduced. We remark that the former two approaches has been independently reported to have a superior performance than the PPE, but not have been yet compared with each other.

3.1 The Poisson Pressure Estimator (PPE)

The PPE, in the context of finite elements, is based on the assumption that the pressure gradient $\boldsymbol{\nabla} p$ satisfies a weak version of Equation (1). Hence, the estimated relative pressure at time $t^{n+1/2} := (t^n + t^{n+1})/2$ can be found as a solution of the following problem: Find $p_{\text{ppe}}^{n+1/2} \in \mathcal{P}_{1,h}$ such that

$$\int_\Omega \boldsymbol{\nabla} p_{\text{ppe}}^{n+1/2} \cdot \boldsymbol{\nabla} q = -\frac{\rho}{\tau} \int_\Omega (\boldsymbol{u}_m^{n+1} - \boldsymbol{u}_m^n) \cdot \boldsymbol{\nabla} q - \rho \int_\Omega (\boldsymbol{u}_m^{n+1/2} \cdot \boldsymbol{\nabla} \boldsymbol{u}_m^{n+1/2}) \cdot \boldsymbol{\nabla} q \tag{3}$$

for all $q \in \mathcal{P}_{1,h}$, and $p_{\text{ppe}} = q = 0$ on Γ_o.

Note that we leave out the term $\Delta \boldsymbol{u}_m$ since it was reported in [9] that the viscous part of the pressure gradient in large vessels is negligible, what we confirm in our numerical experience. Moreover, since $\boldsymbol{u}_m \in \mathcal{P}_{1,h}$, the data does not posses enough regularity to compute its laplacian.

Then, the pressure drop at time $t^{n+1/2}$ between the outlet and the inlet is evaluated with Equation (2) using $p_{\text{ppe}}^{n+1/2}$. Note also that the midpoint time evaluation scheme allows a second order approximation with respect to time and to reduce the noise variance of the measurements $\boldsymbol{u}_m^{n+1/2}$ by a factor of 2 with respect to the original variance of the measurements $\boldsymbol{u}_m^n$.

3.2 The Stokes estimator (STE)

The STE formulated in [11] consists in perturbing the Navier–Stokes equation with the Laplacian of an auxiliar divergence-free velocity field $\boldsymbol{w}$. This leads to a mixed problem for the pressure, in terms of the measured velocity, instead of a Poisson problem as in the PPE.

Defining $\mathcal{P}_{1,h}^b$ as the finite element space with linear piecewise polinimials with an additional bubble function at the centroid of the element, the STE is formulated as follows for the time step $t^{n+1/2}$: Find $\boldsymbol{w} \in [\mathcal{P}_{1,h}^b]^d$ and $p_{ste}^{n+1/2} \in \mathcal{P}_{1,h}$, such that

$$\begin{aligned} \int_\Omega \boldsymbol{\nabla} \boldsymbol{w} : \boldsymbol{\nabla} \hat{\boldsymbol{w}} - \int_\Omega p_{ste}^{n+1/2} (\boldsymbol{\nabla} \cdot \hat{\boldsymbol{w}}) + \int_\Omega (\boldsymbol{\nabla} \cdot \boldsymbol{w}) q \;\; &= \;\; -\frac{\rho}{\tau} \int_\Omega (\boldsymbol{u}_m^{n+1} - \boldsymbol{u}_m^n) \cdot \hat{\boldsymbol{w}} \\ &\quad -\rho \int_\Omega (\boldsymbol{u}_m^{n+1/2} \cdot \boldsymbol{\nabla} \boldsymbol{u}_m^{n+1/2}) \cdot \hat{\boldsymbol{w}} \end{aligned} \tag{4}$$

for all $\hat{\boldsymbol{w}} \in [\mathcal{P}_{1,h}^b]^d$ and $q \in \mathcal{P}_{1,h}$, with $\boldsymbol{w} = \hat{\boldsymbol{w}} = \boldsymbol{0}$ on Γ. Then, the pressure drop at time $t^{n+1/2}$ between the outlet and the inlet is evaluated with Formula (2) using $p_{\text{ste}}^{n+1/2}$. We remark here that since we are only interested in relative pressures, no additional information on the pressure field $p_{ste}^{n+1/2}$ is needed for ensuring solvability of Problem (4). Note also that, as for the PPE, the viscous term is neglected.

3.3 The work-energy relative pressure estimator (WERP)

The starting point of the formulation of the WERP method introduced in [4] is the classical energy relation of an incompressible Newtonian fluid, which can be obtained either by writing the conservation law for the energy density $\rho \boldsymbol{u}^2/2$ directly or multiplying (1) by $\boldsymbol{u}$ and integrating over Ω. This relation reads

$$\frac{\rho}{2}\int_\Omega \partial_t(|\boldsymbol{u}|^2) + \frac{\rho}{2}\int_\Gamma (\boldsymbol{u}\cdot\boldsymbol{n})|\boldsymbol{u}|^2 + \mu\int_\Omega |\boldsymbol{\nabla u}|^2 + \int_\Gamma p\,(\boldsymbol{u}\cdot\boldsymbol{n}) - \mu\int_\Gamma (\boldsymbol{\nabla u}\cdot\boldsymbol{n})\cdot\boldsymbol{u} = 0\ . \quad (5)$$

with $|\cdot|$ denoting the Euclidian norm.

The WERP is then formulated by assuming that: (i) the measurements $\boldsymbol{u}_m^n$ satisfy relation (5), (ii) $\boldsymbol{u}_m^n\cdot\boldsymbol{n} \approx 0$ on Γ_w (i.e. the vessel walls nearly don't move), (iii) the viscous forces on Γ are negligible, (iv) and the pressure is nearly constant on Γ_i and Γ_o. Doing so, the WERP pressure estimator at time $t^{n+1/2}$ is written as:

$$\delta p_{werp}^{n+1/2}(\boldsymbol{u}_m^{n,n+1}) = \frac{-1}{\Lambda(\boldsymbol{u}_m^{n+1/2})}\left(E_{kin}(\boldsymbol{u}_m^{n+1}) - E_{kin}(\boldsymbol{u}_m^n) + E_{conv}(\boldsymbol{u}_m^{n+1/2}) + E_{visc}(\boldsymbol{u}_m^{n+1/2})\right) \quad (6)$$

with

$$E_{kin}(\boldsymbol{w}) = \frac{\rho}{2\tau}\int_\Omega |\boldsymbol{w}|^2 \quad (7)$$

$$E_{conv}(\boldsymbol{w}) = \frac{\rho}{2}\int_{\Gamma_i\cup\Gamma_o} (\boldsymbol{w}\cdot\boldsymbol{n})|\boldsymbol{w}|^2 \quad (8)$$

$$E_{visc}(\boldsymbol{w}) = \mu\int_\Omega |\boldsymbol{\nabla w}|^2 - \mu\int_\Gamma (\boldsymbol{\nabla w}\cdot\boldsymbol{n})\cdot\boldsymbol{w} \quad (9)$$

$$\Lambda(\boldsymbol{w}) = \int_{\Gamma_i} \boldsymbol{w}\cdot\boldsymbol{n}. \quad (10)$$

As it is well known from numerical analysis, the use of the mid-point scheme in (6) does not induce any perturbation compared with the time-continuous energy relation (5), independently on the time step τ.

We can see that this formulation may be unstable at small in-/outflows due to the division by $\Lambda(\boldsymbol{u}_m^{n+1/2})$. In other words, when the inflow is small, perturbations (e.g. due to the noise) can induce large errors in $\Lambda(\boldsymbol{u}_m^{n+1/2})$ leading to an unphysical amplification of the estimated relative pressure. Another relevant issue is that the WERP induces systematic shifts in the pressure curve in the presence of noise, as we will see in the next section. Moreover, the WERP can only by construction estimate relative pressure in geometries with only one inflow and one outflow, due to the assumption $\boldsymbol{u}_m^n\cdot\boldsymbol{n} \approx 0$ on Γ_w needed to eliminate the pressure field on Γ_w out of the formulation.

4 New estimation methods

In this section we present new pressure estimation methods, inspired from the state-of-the-art approaches, and we will see later in the numerical examples that they can lead to

improvements in the estimation results.

4.1 The integrated STE (STEint)

We propose to modify the STE method originally proposed in [11] and formulated in Equation (4) by taking advantage of the regularity of the auxiliar velocity field and integrating by parts the convective and viscous term.

The STEint is formulated as follows for the time step $t^{n+1/2}$. Find $\boldsymbol{w} \in [\mathcal{P}^b_{1,h}]^d$ and $p^{n+1/2}_{stei} \in \mathcal{P}_{1,h}$, such that

$$\begin{aligned}\int_\Omega \boldsymbol{\nabla w} : \boldsymbol{\nabla \hat{w}} - \int_\Omega p^{n+1/2}_{stei}(\boldsymbol{\nabla}\cdot\boldsymbol{\hat{w}}) + \int_\Omega (\boldsymbol{\nabla}\cdot\boldsymbol{w})q \;\; &= \;\; -\frac{\rho}{\tau}\int_\Omega (\boldsymbol{u}^{n+1}_m - \boldsymbol{u}^n_m)\cdot\boldsymbol{\hat{w}} \\ &\quad +\rho\int_\Omega (\boldsymbol{u}^{n+1/2}_m\cdot\boldsymbol{\nabla\hat{w}})\cdot\boldsymbol{u}^{n+1/2}_m \\ &\quad -\mu\int_\Omega \boldsymbol{\nabla u}^{n+1/2}_m : \boldsymbol{\nabla\hat{w}} \qquad (11)\end{aligned}$$

for all $\boldsymbol{\hat{w}} \in [\mathcal{P}^b_{1,h}]^d$ and $q \in \mathcal{P}_{1,h}$, with $\boldsymbol{w} = \boldsymbol{\hat{w}} = \boldsymbol{0}$ on Γ.

Note that the boundary terms of the integration by parts do not appear since $\boldsymbol{\hat{w}} = \boldsymbol{0}$. We point out that this integration by parts is not straightforward for the PPE method due to the lack of enough regularity of $\boldsymbol{\nabla} q$ in Equation (3) when standard piecewise polynomial finite element spaces are used (like $\mathcal{P}_{1,h}$).

Then, the pressure drop at time $t^{n+1/2}$ between the outlet and the inlet is evaluated with Formula (2) using $p^{n+1/2}_{\text{stei}}$.

4.2 The Darcy estimator (DAE)

Note that, a similar alternative for the STE would be to use a Darcy formulation for $\boldsymbol{w}$ instead of Stokes. Let $\mathcal{RT}^k_h$ be the usual Raviart-Thomas finite element space of degree k. Then, find $\boldsymbol{w} \in \mathcal{RT}^1_h$ and $p^{n+1/2}_{\text{dae}} \in \mathcal{P}_{1,h}$, such that

$$\begin{aligned}\int_\Omega \boldsymbol{w}\cdot\boldsymbol{\hat{w}} - \int_\Omega p^{n+1/2}_{\text{dae}}(\boldsymbol{\nabla}\cdot\boldsymbol{\hat{w}}) + \int_\Omega (\boldsymbol{\nabla}\cdot\boldsymbol{w})q \;\; &= \;\; -\frac{\rho}{\tau}\int_\Omega (\boldsymbol{u}^{n+1}_m - \boldsymbol{u}^n_m)\cdot\boldsymbol{\hat{w}} \\ &\quad -\rho\int_\Omega (\boldsymbol{u}^{n+1/2}_m\cdot\boldsymbol{\nabla u}^{n+1/2}_m)\cdot\boldsymbol{\hat{w}} \\ &\quad +\mu\int_\Omega \Delta\boldsymbol{u}^{n+1/2}_m\cdot\boldsymbol{\hat{w}} \qquad (12)\end{aligned}$$

for all $\boldsymbol{\hat{w}} \in \mathcal{RT}^1_h$ and $q \in \mathcal{P}_{1,h}$, with $\boldsymbol{w}\cdot\boldsymbol{n} = \boldsymbol{\hat{w}}\cdot\boldsymbol{n} = 0$ on Γ. This approach has not yet been reported, to the authors best knowledge. As we will see in the numerical examples this does not yield to better results than the STE, indeed, and will only slightly over perform the PPE. Note also that here the integration by parts of the convective and viscous terms of the right-hand side, as by the STEint, is for formal reasons not possible since $\boldsymbol{\hat{w}} \in \mathcal{H}_{\text{div}}(\Omega)$ and it can be easily shown that $\mathcal{H}_1(\Omega) \subset \mathcal{H}_{\text{div}}(\Omega)$. In fact, tests in three dimensions (not shown here) gave very poor results for such a method.

4.3 Integral momentum relative pressure estimator (IMRP)

In this section we derive a new formulation for the integral relative pressure estimator based on a general class of test functions, and we will analyze it in terms of its bias.

Assume that we have computed a function $\boldsymbol{v}$ in Ω satisfying

$$\boldsymbol{\nabla}\cdot\boldsymbol{v}\approx 0\ ,\ \boldsymbol{v}\cdot\boldsymbol{n}=0 \text{ on } \Gamma_w \tag{13}$$

If we multiply Equation $(1)_1$ by $\boldsymbol{v}$ and we integrate over Ω

$$\underbrace{\rho\int_\Omega \partial_t\boldsymbol{u}\cdot\boldsymbol{v}}_{I_{kin}(\partial_t\boldsymbol{u})}+\underbrace{\rho\int_\Omega(\boldsymbol{u}\cdot\boldsymbol{\nabla}\boldsymbol{u})\cdot\boldsymbol{v}}_{I_{conv}(\boldsymbol{u})}+\underbrace{\int_\Omega\boldsymbol{\nabla}p\cdot\boldsymbol{v}}_{I_{pres}}\underbrace{-\mu\int_\Omega\Delta\boldsymbol{u}\cdot\boldsymbol{v}}_{I_{visc}(\boldsymbol{u})}=0\ . \tag{14}$$

we obtain for each of the terms

$$I_{conv}(\boldsymbol{u}) = -\rho\int_\Omega(\boldsymbol{u}\cdot\boldsymbol{\nabla}\boldsymbol{v})\cdot\boldsymbol{u}+\rho\int_\Gamma(\boldsymbol{u}\cdot\boldsymbol{n})(\boldsymbol{u}\cdot\boldsymbol{v}) \tag{15}$$

$$I_{pres} = -\int_\Omega p(\boldsymbol{\nabla}\cdot\boldsymbol{v})+\int_\Gamma p\,(\boldsymbol{v}\cdot\boldsymbol{n})=\int_{\Gamma_i\cup\Gamma_o}p\,(\boldsymbol{v}\cdot\boldsymbol{n}) \tag{16}$$

$$I_{visc}(\boldsymbol{u}) = \mu\int_\Omega\boldsymbol{\nabla}\boldsymbol{u}:\boldsymbol{\nabla}\boldsymbol{v}-\mu\int_\Gamma(\boldsymbol{\nabla}\boldsymbol{u}\cdot\boldsymbol{n})\cdot\boldsymbol{v} \tag{17}$$

using standard integration by parts.

The integral momentum relative pressure estimator (IMRP) is then formulated by assuming that: (i) the measurements $\boldsymbol{u}_m^n$ satisfy relation (14), (ii) the pressure is nearly constant on Γ_i and Γ_o. Doing so, the IMRP estimator at time $t^{n+1/2}$ is formulated as:

$$\delta p_{\text{imrp}}^{n+1/2}(\boldsymbol{u}_m^{n,n+1})=-\frac{1}{\Lambda(\boldsymbol{v})}\left(I_{kin}(\frac{\boldsymbol{u}_m^{n+1}-\boldsymbol{u}_m^n}{\tau})+I_{conv}(\boldsymbol{u}_m^{n+1/2})+I_{visc}(\boldsymbol{u}_m^{n+1/2})\right)\ . \tag{18}$$

Note that the requirements on the test function in (13) serve only so that the pressure field vanishes (up to the relative pressure) in (16).

Notice also that the integral terms $I_{kin}, I_{conv}, I_{visc}$ are multiplied by $1/\Lambda(\boldsymbol{v})$ in the estimator formulation, which is independent of the measurements. This is an advantage compared to the WERP for the potential spurious amplifications for low flows. Another advantage will be clear after the bias analysis. We also point out that we did not make any assumption on the velocity measurements on the boundary Γ_w, as it was done for the WERP. Hence it is potentially better at capturing the pressure gradient changes due to the wall deformation.

We propose the test function $\boldsymbol{v}$ as the solution of the following Poiseuille flow, i.e. a Stokes flow solution with unitary Neumann load on Γ_i: Find $\boldsymbol{v}\in[\mathcal{P}_{1,h}^b]^d$ and $z\in\mathcal{P}_{1,h}$,

$$\int_\Omega\boldsymbol{\nabla}\boldsymbol{v}:\boldsymbol{\nabla}\boldsymbol{\psi}+\int_\Omega z\boldsymbol{\nabla}\cdot\boldsymbol{\psi}+\int_\Omega q\boldsymbol{\nabla}\cdot\boldsymbol{v}+\int_{\Gamma_i}\boldsymbol{\psi}\cdot\boldsymbol{n}=0\ , \tag{19}$$

for all $\boldsymbol{\psi} \in [\mathcal{P}^b_{1,h}]^d$ and $q \in \mathcal{P}_{1,h}$, and with $\boldsymbol{v} = \boldsymbol{\psi} = \mathbf{0}$ on Γ_w. It is not necessary to introduce any coefficient in the viscous term in (19) since the IMRP estimator is independent of any constant scaling of the velocity field, see Equation (18). The same applies to the unitary Neumann load in (19).

We remark that this is not only choice for $\boldsymbol{v}$. Alternatives may be Brinkman or Darcy flows. In several numerical test that we performed no advantage over a simple Poiseuille flow was established in the pressure gradient results. Specifically, the results of the Brinkman flow were dependent on the weighting of the mass term, possibly leading to deteriorated results if this weight was chosen either too large or too small. In the case of a Darcy flow, this is in fact a naive choice due to the lack of regularity of the solutions gradient, which is need in the evaluation of the IMRP in Equation (18). A further option would be to include convective terms for $\boldsymbol{v}$. However, in our numerical experiments, this gave considerably worse approximation results of the IMRP.

Therefore, we do not present any results for additional test functions for the sake of clarity and conciseness.

Remark 1. *The final relative pressure estimation seems to not considerably depend on the order of the finite element space used for the test function in the numerical experiments. Differences between the different spaces can only be appreciated for coarse mesh spacing of the measurements, i.e. larger than* 3 *mm. The same applies to the discretization of the STE, STEint and DAE mixed problems.*

5 Bias analysis

We remind the reader that deal with random and additive perturbation of measured velocity. In this section we detail then how to compute the bias of the estimation methods introduced previously. This implies in practice to calculate the following quantity:

$$\mathbb{E}\left(\delta p^{n+1/2}(\boldsymbol{u}_h^{n,n+1} + \boldsymbol{\varepsilon}^{n,n+1})\right) - \delta p^{n+1/2}(\boldsymbol{u}_h^{n,n+1}) \tag{20}$$

Note that it has not been done in all original works (i.e for PPE, STE and WERP), to the authors best knowledge.

5.1 PPE

Since $\boldsymbol{\varepsilon}^n \in [\mathcal{P}_{1,h}]^d$ is a discrete noise field we can write it (using the Einstein summation convention from now on) as $\boldsymbol{\varepsilon}_i^n(\boldsymbol{x}) = N_j(\boldsymbol{x}) e_{i,j}^n$, with $N_j(\boldsymbol{x})$ the finite element shape function for the j-th degree-of-freedom of $\mathcal{P}_{1,h}$ and i denotes the spatial directions.

Remember also that the degrees-of-freedom $e_{i,j}^n$ are independently identically distributed (i.i.d.) following a normal distribution $\mathcal{N}(0, \sigma^2)$ for all n, i, j. For any linear, differential operator with deterministic coefficients $\mathbb{D} : \mathcal{H}_1(\Omega) \to \mathcal{L}_2(\Omega)$ we have therefore the following identity:

$$\mathbb{E}\left(\int_\Omega \mathbb{D}(\boldsymbol{\varepsilon}_i^n)\right) = \int_\Omega \mathbb{E}\left(e_{i,j}^n\right) \mathbb{D}(N_j(\boldsymbol{x})) = 0 \tag{21}$$

To compute then the bias (20) for the PPE method we proceed as follows. Note that the function $b_{\text{ppe}} := \mathbb{E}(p_{\text{ppe}}^{n+1/2}(\boldsymbol{u}_m^{n,n+1})) - p_{\text{ppe}}^{n+1/2}(\boldsymbol{u}_h^{n,n+1})$ satisfies the problem: Find $b_{\text{ppe}} \in \mathcal{P}_{1,h}$ such that

$$\begin{aligned}\int_\Omega \boldsymbol{\nabla} b_{\text{ppe}} \cdot \boldsymbol{\nabla} q \;\; = \;\; & \mathbb{E}\left(-\frac{\rho}{\tau}\int_\Omega (\boldsymbol{u}_m^{n+1} - \boldsymbol{u}_m^n)\cdot\boldsymbol{\nabla} q\right) + \frac{\rho}{\tau}\int_\Omega (\boldsymbol{u}_h^{n+1} - \boldsymbol{u}_h^n)\cdot\boldsymbol{\nabla} q \\ & -\mathbb{E}\left(\rho\int_\Omega (\boldsymbol{u}_m^{n+1/2}\cdot\boldsymbol{\nabla}\boldsymbol{u}_m^{n+1/2})\cdot\boldsymbol{\nabla} q\right) + \rho\int_\Omega (\boldsymbol{u}_h^{n+1/2}\cdot\boldsymbol{\nabla}\boldsymbol{u}_h^{n+1/2})\cdot\boldsymbol{\nabla} q\end{aligned} \tag{22}$$

for all $q \in \mathcal{P}_{1,h}$, and $b_{\text{ppe}} = q = 0$ on Γ_o. Since $\boldsymbol{u}_m^n = \boldsymbol{u}_h^n + \boldsymbol{\varepsilon}^n$, the kinetic terms of the right-hand-side of Problem (22) are zero due to identity (21). For the convective terms, the only ones surviving are

$$\begin{aligned}\rho\int_\Omega \mathbb{E}\left((\boldsymbol{\varepsilon}^{n+1/2}\cdot\boldsymbol{\nabla}\boldsymbol{\varepsilon}^{n+1/2})\right)\cdot\boldsymbol{\nabla} q \;\; &= \;\; \rho\int_\Omega \mathbb{E}\left(\boldsymbol{\varepsilon}_k^{n+1/2}\partial_k\boldsymbol{\varepsilon}_i^{n+1/2}\right)\partial_i q \\ &= \;\; \rho\int_\Omega \mathbb{E}\left(N_j e_{k,j}^{n+1/2}\partial_k(N_\ell e_{i,\ell}^{n+1/2})\right)\partial_i q \\ &= \;\; \rho\int_\Omega \mathbb{E}\left(e_{k,j}^{n+1/2}e_{i,\ell}^{n+1/2}\right)N_j\partial_k N_\ell\partial_i q \\ &= \;\; \rho\int_\Omega \frac{\sigma^2}{2}N_j\partial_k N_j\partial_k q = \frac{\rho\sigma^2}{4}\int_\Omega \partial_k\sum_j (N_j)^2\partial_k q \\ &= \;\; \frac{\rho\sigma^2}{4}\int_\Omega \boldsymbol{\nabla}\alpha\cdot\boldsymbol{\nabla} q\end{aligned}$$

with $\alpha = \sum_j (N_j)^2$ in $\mathcal{P}_{2,h}$. Therefore, we can compute the bias spatial distribution b_{ppe} by solving:

$$\int_\Omega \boldsymbol{\nabla} b_{\text{ppe}}\cdot\boldsymbol{\nabla} q = -\frac{\rho\sigma^2}{4}\int_\Omega \boldsymbol{\nabla}\alpha\cdot\boldsymbol{\nabla} q\ . \tag{23}$$

with $b_{\text{ppe}} = q = 0$ on Γ_o. Finally, the bias for the relative pressure δp can be computed by evaluating Formula (2) with b_{ppe} instead of the pressure.

We want to remark that this expression provides a closed form for the bias, depending basically on known constants and the geometry itself, and it is independent of the real velocity field and hence also of time. Therefore, it can be always evaluated a priori and in the numerical examples we will verify that it is absolutely negligible with respect to the relative pressure of interest. This will be also the case with the rest of the methods, except the WERP.

5.2 STE and DAE

Fully analogously to the PPE since they both share the same form for the right-hand-side, the bias of STE and DAE can be computed by solving the following problems.

For the STE: Find $\boldsymbol{w} \in [\mathcal{P}^b_{1,h}]^d$ and $b_{\text{ste}} \in \mathcal{P}_{1,h}$, such that

$$\int_\Omega \boldsymbol{\nabla w} : \boldsymbol{\nabla \hat{w}} - \int_\Omega b_{\text{ste}}(\boldsymbol{\nabla} \cdot \hat{\boldsymbol{w}}) + \int_\Omega (\boldsymbol{\nabla} \cdot \boldsymbol{w}) q \;=\; -\frac{\rho\sigma^2}{4} \int_\Omega \boldsymbol{\nabla}\alpha \cdot \hat{\boldsymbol{w}} \tag{24}$$

for all $\hat{\boldsymbol{w}} \in [\mathcal{P}^b_{1,h}]^d$ and $q \in \mathcal{P}_{1,h}$, with $\boldsymbol{w} = \hat{\boldsymbol{w}} = \boldsymbol{0}$ on Γ.

And now for the DAE: Find $\boldsymbol{w} \in \mathcal{RT}^1_h$ and $b_{\text{dae}} \in \mathcal{P}_{1,h}$, such that

$$\int_\Omega \boldsymbol{w} \cdot \hat{\boldsymbol{w}} - \int_\Omega b_{\text{dae}}(\boldsymbol{\nabla} \cdot \hat{\boldsymbol{w}}) + \int_\Omega (\boldsymbol{\nabla} \cdot \boldsymbol{w}) q \;=\; -\frac{\rho\sigma^2}{4} \int_\Omega \boldsymbol{\nabla}\alpha \cdot \hat{\boldsymbol{w}} \tag{25}$$

for all $\hat{\boldsymbol{w}} \in \mathcal{RT}^1_h$ and $q \in \mathcal{P}_{1,h}$, with $\boldsymbol{w} \cdot \boldsymbol{n} = \hat{\boldsymbol{w}} \cdot \boldsymbol{n} = 0$ on Γ.

5.3 STEint

Due to the integration by parts in the right-hand-side, the STEint case has to be handled slightly different. Again, due to identity (21) the kinetic, and now also the viscous terms in the right-hand-side of the bias equation, vanish. The only surviving term in the convective part has the form:

$$\begin{aligned} \rho \int_\Omega \mathbb{E}\left((\boldsymbol{\varepsilon}^{n+1/2} \cdot \boldsymbol{\nabla}\hat{\boldsymbol{w}}) \cdot \boldsymbol{\varepsilon}^{n+1/2}\right) &= \rho \int_\Omega \mathbb{E}\left(\boldsymbol{\varepsilon}_i^{n+1/2} \partial_i \hat{\boldsymbol{w}}_j \boldsymbol{\varepsilon}_j^{n+1/2}\right) \\ &= \rho \int_\Omega \mathbb{E}\left(e_{i,k}^{n+1/2} e_{j,\ell}^{n+1/2}\right) N_k N_\ell \partial_i \hat{\boldsymbol{w}}_j = \frac{\rho\sigma^2}{2} \int_\Omega \alpha \boldsymbol{\nabla} \cdot \hat{\boldsymbol{w}} \end{aligned} \tag{26}$$

Therefore, for the STEint the bias equation reads: Find $\boldsymbol{w} \in [\mathcal{P}^b_{1,h}]^d$ and $b_{\text{stei}} \in \mathcal{P}_{1,h}$, such that

$$\int_\Omega \boldsymbol{\nabla w} : \boldsymbol{\nabla \hat{w}} - \int_\Omega b_{\text{stei}}(\boldsymbol{\nabla} \cdot \hat{\boldsymbol{w}}) + \int_\Omega (\boldsymbol{\nabla} \cdot \boldsymbol{w}) q \;=\; \frac{\rho\sigma^2}{2} \int_\Omega \alpha \boldsymbol{\nabla} \cdot \hat{\boldsymbol{w}} \tag{27}$$

for all $\hat{\boldsymbol{w}} \in [\mathcal{P}^b_{1,h}]^d$ and $q \in \mathcal{P}_{1,h}$, with $\boldsymbol{w} = \hat{\boldsymbol{w}} = \boldsymbol{0}$ on Γ.

5.4 IMRP

The bias of the IMRP can be directly defined as

$$b_{\text{irmp}} = \mathbb{E}(\delta p^{n+1/2}_{\text{imrp}}(\boldsymbol{u}^{n,n+1}_m)) - \delta p^{n+1/2}_{\text{imrp}}(\boldsymbol{u}^{n,n+1}_h)$$

It can be easily verified that due to the identity (21) the bias expression reduces to convective terms only:

$$\begin{aligned} b_{\text{irmp}} &= -\frac{1}{\Lambda(\boldsymbol{v})}\left(-\rho \int_\Omega \mathbb{E}\left(\boldsymbol{\varepsilon}_i^{n+1/2} \partial_j \boldsymbol{v}_i \boldsymbol{\varepsilon}_j^{n+1/2}\right) + \rho \int_\Gamma \mathbb{E}(\boldsymbol{\varepsilon}_i^{n+1/2} \boldsymbol{n}_i \boldsymbol{\varepsilon}_j^{n+1/2} \boldsymbol{v}_j)\right) \\ &= \frac{\rho\sigma^2}{2\Lambda(\boldsymbol{v})} \int_\Omega \alpha \boldsymbol{\nabla} \cdot \boldsymbol{v} - \frac{\rho}{\Lambda(\boldsymbol{v})} \int_\Gamma N_k N_\ell \boldsymbol{n}_i \boldsymbol{v}_j \mathbb{E}(e_{i,k}^{n+1/2} e_{j,\ell}^{n+1/2}) \\ &= \frac{\rho\sigma^2}{2\Lambda(\boldsymbol{v})} \int_\Omega \alpha \boldsymbol{\nabla} \cdot \boldsymbol{v} - \frac{\rho\sigma^2}{2\Lambda(\boldsymbol{v})} \int_\Gamma \alpha \boldsymbol{v} \cdot \boldsymbol{n} \; . \end{aligned}$$

5.5 WERP

We will now end the bias analysis with the WERP estimator. We will need for the analysis the following additional identities:

$$\mathbb{E}\left(\rho\int_\Omega|\boldsymbol{\varepsilon}^n|^2\right)=\sigma^2\,\mathrm{tr}(\boldsymbol{M}_\Omega),\ \mathbb{E}\left(\mu\int_\Omega|\boldsymbol{\nabla}\boldsymbol{\varepsilon}^{n+1/2}|^2\right)=\frac{\sigma^2}{2}\,\mathrm{tr}(\boldsymbol{K}_\Omega)\ , \tag{28}$$

with $\boldsymbol{M}_\Omega$ and $\boldsymbol{K}_\Omega$ the classical mass and stiffness finite element matrices for the Stokes problem in $\mathcal{P}_{1,h}$, respectively. Then, let us point out that the following identities hold:

The goal is now to compute:

$$b_{\text{werp}}=\mathbb{E}(\delta p^{n+1/2}_{\text{werp}}(\boldsymbol{u}^{n,n+1}_m))-\delta p^{n+1/2}_{\text{werp}}(\boldsymbol{u}^{n,n+1}_h)$$

In order to perform such an analysis, we include an additional assumption that $\Lambda(\boldsymbol{u}^{n+1/2}_m)\approx\Lambda(\boldsymbol{u}^{n+1/2}_h)$, what is reasonable if we are interested in estimating the peak systolic relative pressure, which typically is simultaneous to the peak flow where the signal-to-noise ratio is best.

We proceed therefore as follows:

$$\mathbb{E}(\delta p^{n+1/2}_{werp}(\boldsymbol{u}^{n,n+1}_m))\approx\frac{-1}{\Lambda(\boldsymbol{u}^{n+1/2}_m)}\mathbb{E}\left(E_{kin}(\boldsymbol{u}^{n+1}_m)-E_{kin}(\boldsymbol{u}^n_m)+E_{conv}(\boldsymbol{u}^{n+1/2}_m)+E_{visc}(\boldsymbol{u}^{n+1/2}_m)\right)\ . \tag{29}$$

We now compute separately each term. First the kinetic part

$$\begin{aligned}\mathbb{E}\left(E_{kin}(\boldsymbol{u}^n_m)\right)&=\mathbb{E}\left(\frac{\rho}{2\tau}\int_\Omega|\boldsymbol{u}^n_h+\boldsymbol{\varepsilon}^n|^2\right)\\&=\frac{\rho}{2\tau}\int_\Omega\mathbb{E}\left(|\boldsymbol{u}^n_h|^2+2\boldsymbol{u}^n_h\cdot\boldsymbol{\varepsilon}^n+|\boldsymbol{\varepsilon}^n|^2\right)\\&=E_{kin}(\boldsymbol{u}^n_h)+\frac{\sigma^2}{2\tau}\,\mathrm{tr}(\boldsymbol{M}_\Omega)\ .\end{aligned}$$

Then, the convective part can be reduced using Identity (21):

$$\begin{aligned}\mathbb{E}\left(E_{conv}(\boldsymbol{u}^n_m)\right)&=\frac{\rho}{2}\int_{\Gamma_i\cup\Gamma_o}\mathbb{E}\left(((\boldsymbol{u}^n_h+\boldsymbol{\varepsilon}^n)\cdot\boldsymbol{n})|\boldsymbol{u}^n_h+\boldsymbol{\varepsilon}^n|^2\right)\\&=\frac{\rho}{2}\int_{\Gamma_i\cup\Gamma_o}\mathbb{E}\big((\boldsymbol{u}^n_h\cdot\boldsymbol{n})\left\{|\boldsymbol{u}^n_h|^2+2\boldsymbol{u}^n_h\cdot\boldsymbol{\varepsilon}^n+|\boldsymbol{\varepsilon}^n|^2\right\}\\&\qquad+(\boldsymbol{\varepsilon}^n\cdot\boldsymbol{n})\left\{|\boldsymbol{u}^n_h|^2+2\boldsymbol{u}^n_h\cdot\boldsymbol{\varepsilon}^n+|\boldsymbol{\varepsilon}^n|^2\right\}\big)\\&=E_{conv}(\boldsymbol{u}^n_h)+\frac{\rho}{2}\int_{\Gamma_i\cup\Gamma_o}\mathbb{E}\left((\boldsymbol{u}^n_h\cdot\boldsymbol{n})|\boldsymbol{\varepsilon}^n|^2+2(\boldsymbol{\varepsilon}^n\cdot\boldsymbol{n})(\boldsymbol{u}^n_h\cdot\boldsymbol{\varepsilon}^n)\right)\end{aligned}$$

where it can be easily shown that the very last (cubic) term in the second row vanishes due to the standard result that the cube of a normal variable has also zero expected value. Now

we continue using the fact that $\boldsymbol{\varepsilon}_i^n = N_j e_{i,j}^n$

$$\begin{aligned}
\mathbb{E}\left(E_{conv}(\boldsymbol{u}_m^n)\right) &= E_{conv}(\boldsymbol{u}_h^n) + \frac{\rho}{2}\int_{\Gamma_i\cup\Gamma_o}(\boldsymbol{u}_h^n\cdot\boldsymbol{n})\sum_i \mathbb{E}\left((N_j e_{i,j}^n)^2\right) + 2\mathbb{E}\left((\boldsymbol{\varepsilon}^n\cdot\boldsymbol{n})(\boldsymbol{u}_h^n\cdot\boldsymbol{\varepsilon}^n)\right)\\
&= E_{conv}(\boldsymbol{u}_h^n) + \frac{\rho}{2}\int_{\Gamma_i\cup\Gamma_o}(\boldsymbol{u}_h^n\cdot\boldsymbol{n})(d\sigma^2)\alpha + 2\mathbb{E}\left((N_k e_{i,k}^n)(N_\ell e_{j,\ell}^n)\right)\boldsymbol{n}_i\boldsymbol{u}_{h,j}^n\\
&= E_{conv}(\boldsymbol{u}_h^n) + \frac{\rho}{2}\int_{\Gamma_i\cup\Gamma_o}(\boldsymbol{u}_h^n\cdot\boldsymbol{n})(d\sigma^2)\alpha + 2\sigma^2\alpha\boldsymbol{u}_h^n\cdot\boldsymbol{n}\\
&= E_{conv}(\boldsymbol{u}_h^n) + B_{conv}(\boldsymbol{u}_h^n,\sigma^2)\ ,\ B_{conv}(\boldsymbol{u}_h^n,\sigma^2) = \frac{\rho\sigma^2(d+2)}{2}\int_{\Gamma_i\cup\Gamma_o}(\boldsymbol{u}_h^n\cdot\boldsymbol{n})\alpha
\end{aligned}$$

with d the spatial dimension (in our examples later $d=3$). And at last, the viscous part

$$\begin{aligned}
\mathbb{E}\left(E_{visc}(\boldsymbol{u}_m^{n+1/2})\right) &= E_{visc}(\boldsymbol{u}_h^{n+1/2}) + \mu\int_\Omega 2\boldsymbol{\nabla}\boldsymbol{u}_h^{n+1/2} : \boldsymbol{\nabla}\boldsymbol{\varepsilon}^{n+1/2} + |\boldsymbol{\nabla}\boldsymbol{\varepsilon}^{n+1/2}|^2\\
&= E_{visc}(\boldsymbol{u}_h^{n+1/2}) + \frac{\sigma^2}{2}\operatorname{tr}(\boldsymbol{K}_\Omega)\ .
\end{aligned}$$

Now, we inserted the computed expected values into Equation (29) and we then obtain the following expression for the bias of the WERP estimator

$$b_{\text{werp}} \approx \frac{-1}{\Lambda(\boldsymbol{u}_m^{n+1/2})}\left(\frac{1}{2}B_{conv}(\boldsymbol{u}_h^{n+1/2},\sigma^2) + \frac{\sigma^2}{2}\operatorname{tr}(\boldsymbol{K}_\Omega)\right)\ . \tag{30}$$

Note that B_{conv} depends on both real (unknown) spatially subsampled velocity $\boldsymbol{u}_h^{n+1/2}$ and noise variance σ^2, while the second term of the bias depends on σ^2 and the geometry Ω only. However, we will show in the examples that this term is very small B_{conv} compared with the viscous part of the bias.

Remark 2. *It is not obvious to perform similar computations for the variance of the estimators. For the PPE,STE, STEint and DAE, no expression or equation (to our knowledge) can be formulated. For the WERP and IMRP, even though the expressions for the pressure drop are explicit, in the variance the expected value of the multiplication of integrals containing the noise is needed. This can not be computed as before since these integrals are not i.i.d.*

6 Numerical examples

6.1 Forward simulations

The synthetic measurements are obtained from a Navier-Stokes simulation in a three-dimensional geometry representing an stenotic blood vessel, as shown in Figure 1. The inlet and outlet radius are 1 cm and the stenosis has a radius of 0.4 cm, i.e. 60 % of coarctation. The physical parameters were chosen as $\mu = 0.035$ Poise and $\rho = 1.0\ \text{gr/cm}^3$. An

homogeneous Neumann load on Γ_o was imposed, while an homogeneous Dirichlet condition on Γ_w and the following Dirichlet condition on Γ_i are considered:

$$\boldsymbol{u} = 60(x^2 + z^2 - 1)\sin\left(\frac{5\pi}{2}t\right)\boldsymbol{n} \quad \text{on } \Gamma_w \tag{31}$$

leading to a peak inflow rate and pressure drop of 94 cm^3/s and 21 mmHg, respectively. This pressure drop is typical from transitional coarctations from mild to severe and represents a typical threshold for clinical decisions [14].

The numerical solution of the reference problem was performed using a monolithic velocity-pressure coupling. The space-semidiscretization was performed with $\mathcal{P}^b_{1,h}/\mathcal{P}_{1,h}$ finite elements for the velocity and pressure, respectively, with a mesh spacing of $h = 0.06$ cm. A backward Euler scheme was used for the time-semidiscretization with time-step of 0.002 s, with a semi-implicit treatment of the convective term, and including a Temam stabilization term to ensure Lyapunov stability of the solution in time [12]. At that spatial refinement level, no volume or backflow convective instabilities were observed, so no volume convective or backflow stabilization terms were included in order to not perturb the original equation, e.g. SUPG [3] or backflow stabilization [2].

6.2 Synthetic measurements

Synthetic measurements (see Figure 2) are generated considering the following realistic perturbations of the data:

- An additive Gaussian noise [1], with standard deviation chosen as 10% of the peak velocity for all velocity components as it is usually done in clinical Phase-Contrast imaging adjusting the expected peak velocity (called *VENC* parameter) [5].
- A time subsampling of 0.02 s.
- A spatial subsampling of 0.1, 0.15, 0.2 and 0.25 cm.

6.3 Weighting functions for IMRP

We will use a Poiseuille flow as test functions for the IMRP method (IMRP), that can be appreciated in Figure 3.

6.4 Bias of the estimators

As we remarked in Section 5, we can compute a priori the bias for all methods, which on the geometry on the variance of the noise of the velocity measurements, see Table 1. Only in the case of the WERP, the bias coming from the convective term needs to be computed from the ground truth. However, we show that for small mesh spacing it is reduced and hence the bias of the WERP is controlled by the viscous part.

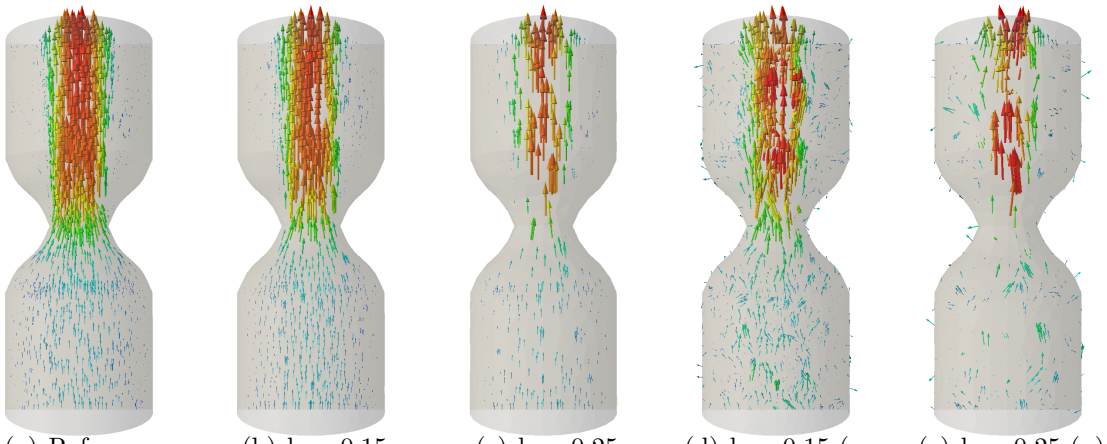

(a) Reference (b) h = 0.15 (c) h = 0.25 (d) h = 0.15 (n (e) h = 0.25 (n)

Figure 2: (a)Reference simulated velocity field (with $h = 0.06$ cm and mini-elements). (b)-(c) Spatially subsampled measurements at time $t = 0.25$ s (noise free). (d)-(e) Spatially subsampled and noisy (n) measurements at time $t = 0.25$.

Note that bias for the STE, STEint and DAE the bias are of the order of the machine precision, while for the PPE is also very small. The IMRP turns to give also a completely negligible bias.

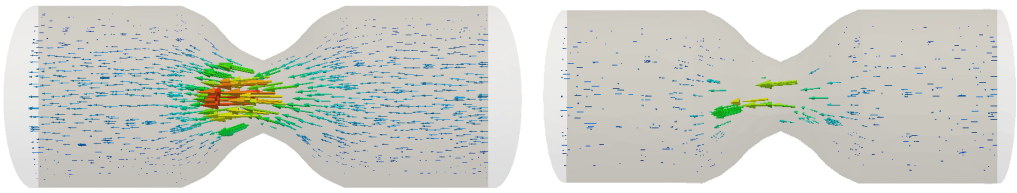

(a) $h = 0.15$ cm (b) $h = 0.25$ cm

Figure 3: Poiseuille test functions for IMRP for different spatial resolutions.

h [cm]	0.1	0.15	0.2	0.25
PPE	$5.7e-13$	$2.1e-13$	$1.4e-13$	$1.0e-13$
STE	$-1.6e-16$	$-1.0e-16$	$-1.6e-16$	$-1.6e-16$
STEint	$1.0e-17$	$8.6e-17$	$7.8e-17$	$-2.4e-17$
DAE	$3.3e-17$	$1.7e-16$	$7.0e-17$	$-9.6e-18$
WERP	2.3	0.9	0.6	0.5
WERP(visc)	2.3	1.0	0.3	1.1
IMRP	$4.2e-06$	$-5.1e-06$	$-7.9e-06$	$-4.1e-08$

Table 1: Computations of the bias [mmHg] for 10% noise in the velocity.

6.5 Estimation results: noise-free measurements

We first study the sensitivity of the relative pressure estimation to the spatial subsampling of the measurements, without any random noise. The results are shown in Figure 4, and the error convergence curves with respecto to h are shown in Figure 5. Note that the best methods turn out finally to be the IMRP and STEint, with the former giving a slightly better precision. They turn out to be very robust when subsampling the measurements compared with the state of the art methods, i.e. PPE, STE and WERP. Note that the PPE, which is the oldest and the most spread approach, was consistently the worst method, in line with the findings of [11, 4]. We also want to remark that the temporal subsampling at this realistic level does not have a considerable impact on the estimation precision, compared with the spatial subsampling, and hence only the time-subsampled results are shown for the sake of conciseness.

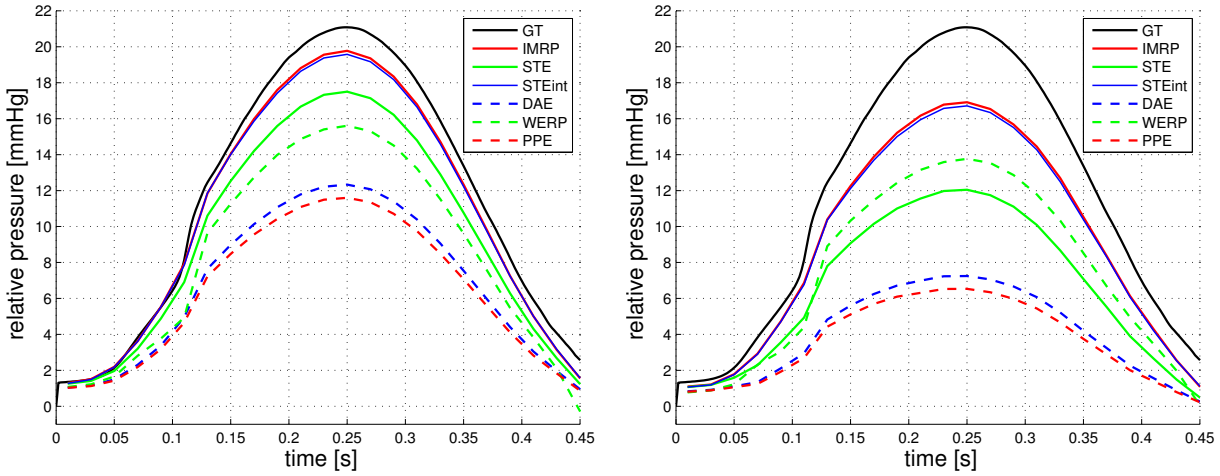

(a) $h = 0.15$ cm (b) $h = 0.25$ cm

Figure 4: Reference ground-truth (GT) and noise-free relative pressure estimations for two different spatial subsampling resolutions including temporal subsampling of 0.02 s.

6.6 Estimation results: noisy measurements

Now we summarize the results with noisy measurements, for which we consider 100 random realizations. The standard deviations of the estimation and the error of the mean with respect to the ground truth (both at peak systole) are presented in Figure 6 and 7. Note that both diminish with the spatial discretization size h for all methods. In addition, by comparing Figures 4 and 6 we verify that the bias is imperceptible, consistently with the values computed a priori in Table 1. As expected, the only exception is the WERP.

As expected due to the "squaring" of the measurements, the method with highest variance is the WERP, while the methods delivering sharper standard deviations are PPE and DAE.

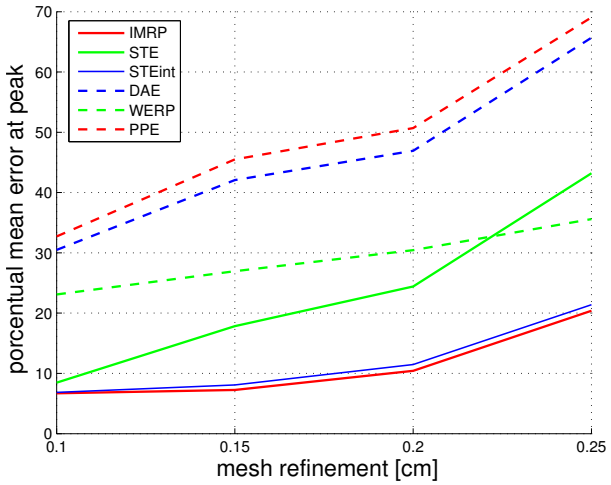

Figure 5: Error of estimation with respect to the ground truth at peak systole for noise-free but spatial subsampled measurements.

However, the differences in standard deviations among all methods are around 1.0 mmHg, meaning around 2.0 mmHg for a 95% confidence interval.

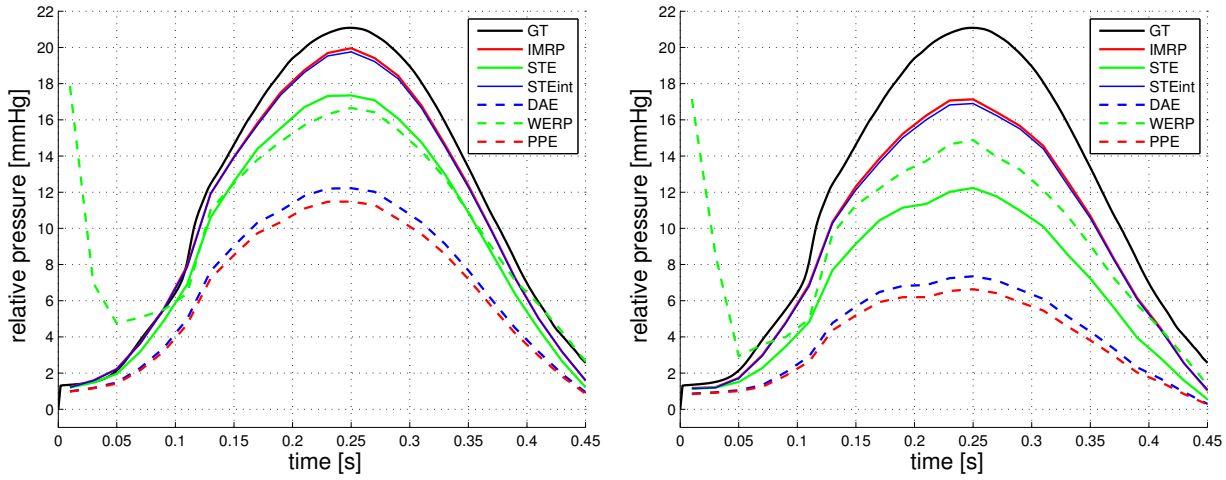

(a) $h = 0.15$ cm (b) $h = 0.25$ cm

Figure 6: Mean pressure estimations with noisy measurements.

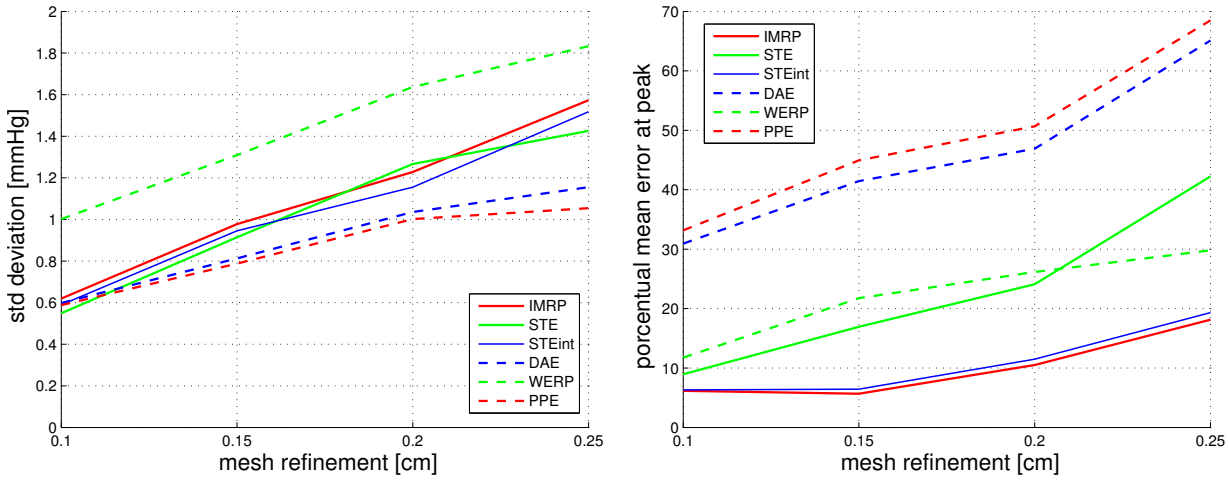

(a) Standard deviation

(b) Mean error

Figure 7: Estimation results at peak systole with noisy measurements.

7 Conclusions

In this work we reviewed, improved, analyzed (both theoretically and numerically) and compared old and recent approaches for estimating relatives pressures from 4D flow data. Consistent with very recent findings, the worst performance was found the be of the classical and widely spread PPE method in terms of its robustness the spatial subsampling.

The WERP method recently introduced in [4], even though the computationally cheapest, it is more sensitive to noise, delivering biased estimations and with larger variances than the other methods.

We also performed computations for the STE method also recently introduced in [11], confirming the that it performs better than the PPE. However, it also presented an important sensitivity when the measurements are subsampled in space. We found out that just a simple integration by parts, in particular of the convective term, considerably reduces this sensitivity. This was not shown in the original article [11]. In this context, we investigate an alternative to the STE method based on the Darcy flow, that we called DAE, obtaining slightly better results than the PPE but worse than the rest of the approaches in terms of estimated mean.

Finally, inspired from the WERP we proposed a new approach based on an integral momentum balance weighted by a simple Poiseuille solution. This turns out to be the best performant method together with the STEint, both in terms of estimated mean and variance, with a low sensitivity to spatial subsampling in current clinical ranges of voxel size used for 4D flow acquisitions.

Summarizing, based on the numerical experiments presented in this work, the methods of choice would be the IMRP and/or the STEint, both newly introduced in our contribution. While the STEint has the advantage of given the full spatial distribution of the pressure

(relative to some point), the IMRP is computationally cheaper when many the relative pressure needs to be computed at many time samples. Therefore, future work will consist on validating these approaches using real 4D flow data and catheter measurements.

Acknowledgements

We sincerely thank discussions with Alfonso Caiazzo and Alexander Linke from WIAS Berlin about finite element discretizations, and with Sergio Uribe and Joaquín Mura from the Center for Biomedical Imaging of the Universidad Católica de Chile about Phase-Contrast MRI.

References

[1] Paul Bao and Lei Zhang. Noise reduction for magnetic resonance images via adaptive multiscale products thresholding. *Medical Imaging, IEEE Transactions on*, 22(9):1089–1099, 2003.

[2] Cristóbal Bertoglio and Alfonso Caiazzo. A Stokes-residual backflow stabilization method applied to physiological flows. *Journal of Computational Physics*, 313:260–278, 2016.

[3] Alexander N Brooks and Thomas JR Hughes. Streamline upwind/Petrov-Galerkin formulations for convection dominated flows with particular emphasis on the incompressible Navier-Stokes equations. *Computer methods in applied mechanics and engineering*, 32(1):199–259, 1982.

[4] Fabrizio Donati, C Alberto Figueroa, Nicolas P Smith, Pablo Lamata, and David A Nordsletten. Non-invasive pressure difference estimation from PC-MRI using the work-energy equation. *Medical Image Analysis*, 26(1):159–172, 2015.

[5] Petter Dyverfeldt, Malenka Bissell, Alex J Barker, Ann F Bolger, Carl-Johan Carlhäll, Tino Ebbers, Christopher J Francios, Alex Frydrychowicz, Julia Geiger, Daniel Giese, et al. 4D flow cardiovascular magnetic resonance consensus statement. *Journal of Cardiovascular Magnetic Resonance*, 17(1):1–19, 2015.

[6] Tino Ebbers and Gunnar Farnebäck. Improving computation of cardiovascular relative pressure fields from velocity MRI. *Journal of Magnetic Resonance Imaging*, 30(1):54–61, 2009.

[7] Tino Ebbers, Lars Wigström, Ann F Bolger, Jan Engvall, and Matts Karlsson. Estimation of relative cardiovascular pressures using time-resolved three-dimensional phase contrast MRI. *Magnetic resonance in medicine*, 45(5):872–879, 2001.

[8] Sebastian BS Krittian, Pablo Lamata, Christian Michler, David A Nordsletten, Jelena Bock, Chris P Bradley, Alex Pitcher, Philip J Kilner, Michael Markl, and Nic P Smith. A finite-element approach to the direct computation of relative cardiovascular pressure from time-resolved MR velocity data. *Medical image analysis*, 16(5):1029–1037, 2012.

[9] Pablo Lamata, Alex Pitcher, Sebastian Krittian, David Nordsletten, Malenka M Bissell, Thomas Cassar, Alex J Barker, Michael Markl, Stefan Neubauer, and Nicolas P Smith. Aortic relative pressure components derived from four-dimensional flow cardiovascular magnetic resonance. *Magnetic resonance in medicine*, 72(4):1162–1169, 2014.

[10] Michael Markl, Alex Frydrychowicz, Sebastian Kozerke, Mike Hope, and Oliver Wieben. 4D flow MRI. *Journal of Magnetic Resonance Imaging*, 36(5):1015–1036, 2012.

[11] H Švihlová, J Hron, J Málek, KR Rajagopal, and K Rajagopal. Determination of pressure data from velocity data with a view toward its application in cardiovascular mechanics. Part 1. Theoretical considerations. *International Journal of Engineering Science*, 2016, In press.

[12] Roger Temam. Une méthode d'approximation de la solution des équations de navier-stokes. *Bulletin de la Société Mathématique de France*, 96:115–152, 1968.

[13] Alec Vahanian, Ottavio Alfieri, Felicita Andreotti, Manuel J. Antunes, Gonzalo Barón-Esquivias, Helmut Baumgartner, Michael Andrew Borger, Thierry P. Carrel, Michele De Bonis, Arturo Evangelista, Volkmar Falk, Bernard Iung, Patrizio Lancellotti, Luc Pierard, Susanna Price, Hans-Joachim Schäfers, Gerhard Schuler, Janina Stepinska, Karl Swedberg, Johanna Takkenberg, Ulrich Otto Von Oppell, Stephan Windecker, Jose Luis Zamorano, Marian Zembala, , Jeroen J. Bax, Helmut Baumgartner, Claudio Ceconi, Veronica Dean, Christi Deaton, Robert Fagard, Christian Funck-Brentano, David Hasdai, Arno Hoes, Paulus Kirchhof, Juhani Knuuti, Philippe Kolh, Theresa McDonagh, Cyril Moulin, Bogdan A. Popescu, Željko Reiner, Udo Sechtem, Per Anton Sirnes, Michal Tendera, Adam Torbicki, Alec Vahanian, Stephan Windecker, , Bogdan A. Popescu, Ludwig Von Segesser, Luigi P. Badano, Matjaž Bunc, Marc J. Claeys, Niksa Drinkovic, Gerasimos Filippatos, Gilbert Habib, A. Pieter Kappetein, Roland Kassab, Gregory Y.H. Lip, Neil Moat, Georg Nickenig, Catherine M. Otto, John Pepper, Nicolo Piazza, Petronella G. Pieper, Raphael Rosenhek, Naltin Shuka, Ehud Schwammenthal, Juerg Schwitter, Pilar Tornos Mas, Pedro T. Trindade, and Thomas Walther. Guidelines on the management of valvular heart disease (version 2012). *European Heart Journal*, 33(19):2451–2496, 2012.

[14] C.A. Warnes, R.G. Williams, T.M. Bashore, J.S. Child, H.M. Connolly, J.A. Dearani, P. del Nido, J.W. Fasules, T.P. Graham, Z.M. Hijazi, S.A. Hunt, M.E. King, M.J. Landzberg, P.D. Miner, M.J. Radford, E.P. Walsh, and G.D. Webb. ACC/AHA 2008 Guidelines for the Management of Adults with Congenital Heart Disease: a report of the American College of Cardiology/American Heart Association Task Force on Practice

Guidelines (writing committee to develop guidelines on the management of adults with congenital heart disease). *Circulation*, 118(1):714–833, 2008.

[15] Carole A Warnes, Roberta G Williams, Thomas M Bashore, John S Child, Heidi M Connolly, Joseph A Dearani, Pedro del Nido, James W Fasules, Thomas P Graham, Ziyad M Hijazi, et al. ACC/AHA 2008 guidelines for the management of adults with congenital heart disease. *Journal of the American College of Cardiology*, 52(23):e143–e263, 2008.